JSE Journal of Systematics and Evolution

doi: 10.1111/jse.12433

Research Article

Congruent species delimitation of two controversial gold-thread nanmu tree species based on morphological and restriction site-associated DNA sequencing data

Xin Ding[1,2], Jian Hua Xiao[1,2], Lang Li[1], John G. Conran[3], and Jie Li[1]*

[1]Plant Phylogenetics and Conservation Group, Centre for Integrative Conservation, Xishuangbanna Tropical Botanical Garden, Chinese Academy of Sciences, Kunming 650223, China

[2]University of Chinese Academy of Sciences, Beijing 100049, China

[3]School of Biological Sciences and Australian Centre for Evolutionary Biology and Biodiversity and Sprigg Geobiology Centre, University of Adelaide, Adelaide, South Australia SA 5005, Australia

*Author for correspondence. E-mail: jieli@xtbg.ac.cn. Tel.: 86-871-6514-4431. Fax: 86-871-6516-0916.

Received 10 November 2017; Accepted 1 May 2018; Article first published online xx Month 2018

Abstract Species delimitation is fundamental to conservation and sustainable use of economically important forest tree species. However, the delimitation of two highly valued gold-thread nanmu species (*Phoebe bournei* (Hemsl.) Yang and *P. zhennan* S. K. Lee & F. N. Wei) has been confusing and debated. To address this problem, we integrated morphology and restriction site-associated DNA sequencing (RAD-seq) to define their species boundaries. We obtained consistent results from the two datasets, supporting two distinct lineages corresponding to *P. bournei* and *P. zhennan*. In *P. bournei*, higher order leaf venation is more prominent, petioles are thicker, and leaf apex angle is narrower, compared to *P. zhennan*. Both datasets also revealed that the former putative *P. bournei* populations from northeastern Guizhou belong to *P. zhennan*. The two species are now distinct in distributions except in the Wuling Mountains, where they overlap. *Phoebe bournei* occurs mainly in central Fujian, southern Jiangxi, the Nanling Mountains, and the Wuling Mountains, whereas *P. zhennan* is found in the adjoining eastern regions of the Qionglai Mountains, the southern Sichuan hills, and the Wuling Mountains. The re-delimitation of *P. bournei* and *P. zhennan* and clarification of their ranges provide a better scientific basis guiding the conservation and sustainable utilization of these tree species.

Key words: delimitation, distribution area, gold-thread nanmu, morphological characters, restriction site-associated DNA sequencing (RAD-seq).

1 Introduction

Gold-thread nanmu is a highly valuable timber well-known for its durability, unique special fragrance, and attractive golden colour. It has been used for the manufacture of coffins and construction of palaces and furniture in China since the pre-Qin Dynasty times (before 221 BC). In the late feudalism period, timber from gold-thread nanmu was supplied exclusively to the imperial court with the name "Emperor Wood" (Cheng, 1983; Li et al., 2004; Chen, 2013). The main sources for gold-thread nanmu are species of *Phoebe* Nees (Lauraceae) from subtropical China, with four of them being the most valuable due to their large size: *P. bournei* (Hemsl.) Yang, *P. chekiangensis* C. B. Shang, *P. hui* Cheng ex Yang, and *P. zhennan* S. K. Lee & F. N. Wei, although the use of *P. neurantha* (Hemsl.) Gamble and *P. sheareri* (Hemsl.) Gamble were also reported (Li et al., 1982, 2008). Among these taxa, *P. bournei* and *P. zhennan* have been regarded as the best sources due to their tall and thick trunks (ca. 20 m tall and 80 cm diameter at breast height) and exceptionally high quality timber (Li et al., 1982; Lin, 1988; Chen, 2013).

Although it is difficult to tell *P. zhennan* from *P. bournei* in the field, they can be distinguished easily from the other *Phoebe* species, and the other gold-thread nanmu *Phoebe* species can also be distinguished readily in morphology. *Phoebe hui* from Sichuan, southern Shanxi, and northeastern Yunnan co-occurs with *P. zhennan*, but the leaf blade of *P. hui* is densely pubescent with gray-white appressed hairs on the lower surface, whereas the leaf lower surface of *P. zhennan* is green. *Phoebe chekiangensis* occurs in northern Fujian, eastern Jiangxi, and northern Zhejiang, overlapping with *P. bournei*, but the leaf of *P. chekiangensis* is usually obovate-elliptic to obovate-lanceolate and 7–17 cm × 3–7 cm in size, whereas that of *P. bournei* is lanceolate or oblanceolate and 7–13 (–15) cm × 2–3 (–4) cm in size. *Phoebe hui* is disjunct from *P. chekiangensis* and easily recognized by its dense gray-white appressed pubescence on leaf lower surface. *Phoebe sheareri* mainly distributes in eastern subtropical China whereas *P. neurantha* mainly occurs in western subtropical China. These two species can be distinguished from the previous four species by their ovoid to ellipsoid-ovoid and smaller fruits

(<1 cm). *Phoebe sheareri* is distinguished from *P. neurantha* by its gray-brown villous leaf pubescence (Li et al., 1982, 2008).

In contrast, the morphological characters traditionally used to separate *P. bournei* and *P. zhennan*, as presently recognized, overlap considerably and the two species also overlap in distributions (Lee et al., 1979; Li et al., 1982, 2008). As a result, the two species cannot be distinguished easily, leading to difficulty in assessment of their distributions, taxonomy, and conservation status. The delimitation of these two putative species has also been a long-running subject of debate as briefly reviewed below (Li et al., 1982, 2008; Zou & Wu, 1997).

Phoebe bournei was originally thought from Sichuan (including Chongqing), Xikang (split into Sichuan and Tibet in 1955), Hubei, and Fujian (Yang, 1945). Lee et al. (1979) subsequently delineated *P. zhennan* to include populations from Sichuan, northwestern Guizhou, and western Hubei using four main morphological characteristics: (i) branchlets densely villous; (ii) leaf blade elliptic; (iii) veinlets abaxially slightly distinct or invisible; and (iv) strongly patent cymose panicles. This taxonomic treatment was followed in both the *Flora Reipublicae Popularis Sinicae* (Li et al., 1982) and *Flora of China* (Li et al., 2008). The authors of both works considered *P. zhennan* to be restricted to Sichuan, northwestern Guizhou, and western Hubei, whereas *P. bournei* occurs in Jiangxi, Fujian, southern Zhejiang, Guangdong, northern Guangxi, Hunan, Hubei, and northeastern and southeastern Guizhou. Zou & Wu (1997) compared these two species morphologically and concluded that their allegedly distinctive characters represented only intraspecific variation, recommending that *P. zhennan* be synonymized under *P. bournei*. However, all studies of this complex to date have been based on limited samples and relatively few characters. As a result, it is difficult to be certain whether there are one or two species involved and, if the latter, how they might be characterized morphologically.

Historically, *P. bournei* and *P. zhennan* were widely distributed elements of the evergreen broad-leaf forests (EBLF) of subtropical China. However, long-term heavy felling, especially in the Ming (1368–1644) and Qing (1644–1912) dynasties, combined with environmental degradation, has resulted in reduction of wild populations, leaving only scattered ancient trees in temples, parks, scenic spots, and villages (Lin, 1988). Both species are listed as Category II protected plants in the Chinese *List of Wild Plants under State Protection I* and as Vulnerable according to the *IUCN Red List of Threatened Species* (IUCN, 2017), *The China Plant Red Data Book* (Fu & Jin, 1991), and the *China Species Red List* (Wang & Xie, 2004).

Accurate species delimitation is essential for effective conservation, but in many reserves in subtropical China populations of *P. bournei* are misidentified as *P. zhennan*, due to the aforementioned problems. In recent studies reporting the utilization and conservation of nanmu, no species identification was provided (Li et al., 2004; Jia et al., 2014).

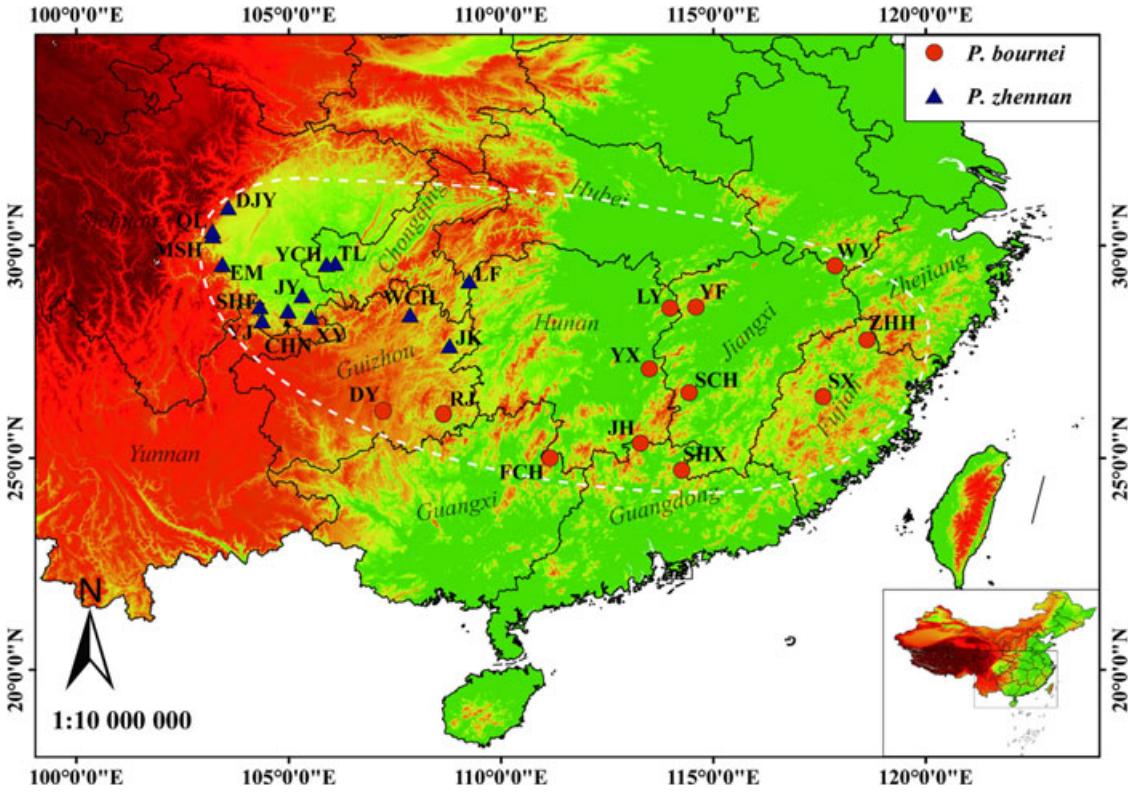

Fig. 1. Distribution of the 26 populations sampled for restriction site-associated DNA sequencing and morphological analyses. The map is from the International Scientific and Technical Data Mirror Site, Computer Network Information Center, Chinese Academy of Sciences (http://www.gscloud.cn). Samples were not identified to species at the time of collection. Orange dots indicate the eastern group (*Phoebe bournei*) and blue triangles indicate the western group (*P. zhennan*) that were identified by phylogenetic and morphological analyses.

There have been no molecular studies comparing *P. bournei* and *P. zhennan*, although there are a few studies examining intraspecific genetic variation (Li et al., 2011; Gao et al., 2016; Song et al., 2017). A molecular study including comprehensive sampling is needed to clarify relationships within the *P. bournei* and *P. zhennan* complex.

Restriction site-associated DNA sequencing (RAD-seq) is a simple and cost-effective technology for sequencing of a reduced genome, especially for non-model species. This technique can produce a vast number of short sequences from various genomic DNA loci and was designed originally as a tool for finding single-nucleotide polymorphisms (SNPs) for population genetic structural inference, linkage mapping, association study, and other intraspecific genomic analyses (Miller et al., 2007; Baird et al., 2008). Recently, RAD-seq has also been used to resolve phylogenetic relationships of diverse lineages including polyploids (e.g., Rubin et al., 2012; Eaton & Ree, 2013; Wagner et al., 2013; Wang et al., 2013; Escudero et al., 2014; Hipp et al., 2014; Takahashi et al., 2014; Qi et al., 2015; Ree & Hipp, 2015; Takahashi & Moreno, 2015; Boucher et al., 2016; Takahashi & Sota, 2016; Fitz-Gibbon et al., 2017; Tripp et al., 2017).

Species distribution is strongly influenced by ecologically limiting factors, especially climatic variables (Woodward, 1987; Pearson et al., 2002; Kozak et al., 2008). Geographic locations of a species' distribution provide critical information on the climatic niche of the species. Clarifying geographic distributions is, therefore, important to understanding the ecological niches of species, which is vital for effective conservation and management of biodiversity.

In this study, we delineated the geographic distribution using occurrence data of herbarium specimens and our field investigation, and undertook analyses of morphological features and RAD-seq data for samples of the *P. bournei* and *P. zhennan* complex, representing their entire distributional areas. Our goals were to elucidate evolutionary relationships within the complex, and determine the climatic variables distinguishing the two species' occurrences. Results of the study are expected to provide a solid scientific basis to guide the conservation management of these valuable timber trees in China.

2 Material and Methods

2.1 Sampling

For morphological analysis, 93 specimens (Table S1) collected from 26 localities (Fig. 1) across the range of *Phoebe bournei* and *P. zhennan* were used. These specimens were processed and deposited in the Herbarium of Xishuangbanna Tropical Botanical Garden (HITBC). For the RAD-seq analyses, we used 26 individuals from the 26 localities that were sampled for morphological study (Table S2). A sample of *Alseodaphnopsis hainanensis* (Merr.) H. W. Li & J. Li was used as the outgroup following Li et al. (2011). Healthy mature leaves were dried in silica gel and stored at 20 °C until processed.

2.2 Morphological analyses

Twenty characters from leaf morphology and one character from branch morphology were used to compare among specimens of putative *P. zhennan* and *P. bournei* (Table S3; Fig. S1). These included the four main characters currently used to separate *P. zhennan* from *P. bournei*, as well other features used to distinguish *Phoebe* species (Lee et al., 1979; Li et al., 1982, 2008). Fifteen characters were continuous (C1–C15), with the remainder (C16–C21) being discrete. Measurements were taken using rulers, Vernier calipers, protractors, and stereomicroscopes. Five randomly selected leaves were measured for the 20 characters and the results averaged for each specimen.

The 21 characters were standardized by mean and standard deviation, then clustered using Ward's method (Milligan, 1980; Takahashi et al., 2014) and ordinated by principal component analysis (PCA) following the Kaiser criterion (Kaiser, 1960). In the PCA, the statistical significance of groups observed in the scatter plot was tested by discriminant analysis of the first three coordinates. The independent sample *t*-test was used to compare intergroup differences. Variation within and between groups was explored with box and whisker plots. All analyses were undertaken with SPSS version 20 (SPSS, Chicago, IL, USA).

2.3 Analyses of RAD-seq data

2.3.1 DNA extraction and RAD library preparation

RNA-free genomic DNA was extracted using a modified CTAB protocol (Rogers & Bendich, 1988) with quality checked by electrophoresis on 1% agarose gels of total DNA solutions

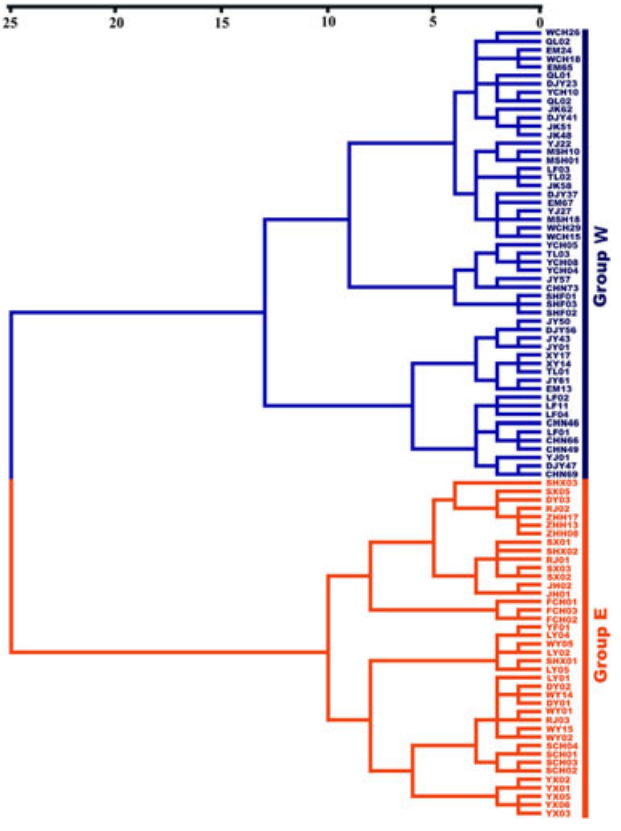

Fig. 2. Result from clustering analysis with Ward's method based on 21 morphological characters of 93 specimens of *Phoebe bournei* (Group E) and *P. zhennan* (Group W) in the study group. Scale bar indicates distance.

adjusted to 30 ng/μL. The RAD-seq libraries were prepared following the protocol described in Etter et al. (2011) with some modifications. Briefly, 1 μg of genomic DNA was digested with the restriction enzyme *Eco*RI (5′-G*AATTC-3′) for 2 h, followed by ligation of Illumina sequencing adaptors (Illumina, San Diego, CA, USA) containing sample-specific barcode sequences to the fragmented DNA using the method of Etter et al. (2011). The fragments were then enriched by polymerase chain reactions. The library preparation and sequencing were carried out by the Beijing Genomics Institute (Shenzhen, China) using Illumina Hiseq 2500.

2.3.2 Processing of RAD-seq data

In the assembly of the RAD-seq data matrix for phylogenetic analyses, two aspects are crucial: identification of orthologous loci across samples and the filtering of orthologous loci according to the number of samples with sequence data for the loci (Rubin et al., 2012). We used PyRAD version 2.0 to process the *de novo* RAD sequences (Eaton, 2014). This software allows for indels when clustering reads into orthologous loci, which is considered an advantage for building phylogenetic data matrices.

In PyRAD, the key parameter for identifying orthologous loci is the clustering threshold (W_{clust}), which controls the minimum proportion of identical nucleotides allowed for identification of orthologous RAD loci within and across samples. When W_{clust} is large, the identification is strict and RAD loci with variable sequences are excluded; when W_{clust} is small, RAD loci from conservative to highly variable sequences can be included, with some misidentification of orthologs. The loci are filtered by choosing the minimum number of taxa (Min_{taxa}) that must recover the sequence of a particular RAD locus. With larger Min_{taxa} values, the matrix contains a higher proportion of RAD loci associated with conserved restriction sites recovered from more taxa while the proportion of missing data decreases and total number of loci also decreases; with smaller Min_{taxa} values, numerous RAD loci recovered from a limited number of taxa are also included. Hence the proportion of missing data increases (Takahashi et al., 2014; Ree & Hipp, 2015).

The raw RAD sequences were sorted by barcode sequences into samples and filtered by removing low-quality reads with a Phred quality score lower than 20 (Q20). Then the barcode sequence and the restriction site were removed from each RAD sequence. Finally, the orthologous RAD loci were identified by W_{clust} and filtered by Min_{taxa} in PyRAD. Four W_{clust} values (55%, 65%, 75%, and 85%) were tested and the matrix with $W_{clust} = 85\%$ was chosen due to its highest number of parsimony informative sites (2 653 576, 2 740 067, 2 754 288, and 2 837 343, respectively), and the $W_{clust} = 85\%$ was equivalent to 15% differences in stacks given the read lengths. Min_{taxa} affects the proportion of missing data in the final matrix, with a trade-off between the proportion of missing data and the number of RAD loci, we used a moderate $Min_{taxa} = 16$ (out of 27 samples) to recover sequences for RAD loci present in 16 or more samples in reconstructing the matrix for phylogenetic analysis. The resulting orthologous loci, including both variable and invariable nucleotides, were concatenated into a supermatrix.

2.3.3 Tree search and evaluation

Maximum likelihood (ML) analysis was carried out for the supermatrix using RAxML version 8.0 (Stamatakis, 2014). A general-time-reversible model with gamma distributed rate variation (GTR + Γ) was chosen because simpler, less inclusive models can greatly reduce the accuracy of phylogenetic

Table 1 Value ranges, mean values, and *t*-test results of 21 morphological characters in the two groups of *Phoebe* species

Character	Group E		Group W		*t*-test
	Range	Mean	Range	Mean	
C1 (Diameter of petiole, cm)	0.091–0.160	0.1249	0.081–0.126	0.1036	$P < 0.0001$
C2 (Length of petiole, cm)	0.710–1.820	1.1611	0.820–2.120	1.3906	$P < 0.0001$
C3 (Length of leaf, cm)	9.560–16.040	12.4716	8.740–15.200	11.661	$P = 0.0236$
C4 (Length of leaf apex, cm)	0.770–2.140	1.2002	0.500–1.740	1.0319	$P = 0.0419$
C5 (Width of middle leaf, cm)	2.274–3.990	3.0361	2.288–4.332	3.1858	$P = 0.0970$
C6 (Width of leaf, cm)	2.274–4.010	3.0726	2.328–4.488	3.2772	$P = 0.0329$
C7 (Length from base to width of leaf, cm)	4.254–8.480	6.4491	4.820–8.900	6.6181	$P = 0.3900$
C8 (Angle of leaf base, °)	36.7–55.8	44.500	29.5–54.8	41.37	$P = 0.0135$
C9 (Angle of leaf apex, °)	42.2–60.9	51.690	50.0–75.4	61.62	$P < 0.0001$
C10 (Number of secondary veins)	8.6–14.4	11.886	9.2–13.6	11.3	$P = 0.0481$
C11 (C3/C6)	3.331–4.877	4.0962	2.609–4.583	3.5943	$P < 0.0001$
C12 (C2/C1)	6.059–14.360	9.3566	7.979–25.090	13.601	$P < 0.0001$
C13 (C7/C3)	0.330–0.579	0.5156	0.500–0.630	0.566	$P < 0.0001$
C14 (C9/C8)	0.841–1.544	1.1891	1.081–2.042	1.5207	$P < 0.0001$
C15 (C4/C3)	0.064–0.150	0.0958	0.043–0.129	0.0884	$P = 0.1817$
C16 (Resolution of tertiary veins)	2.0–3.0	2.7	1.0–3.0	1.8	$P < 0.0001$
C17 (Resolution of quaternary veins)	1.2–3.0	1.9	0.0–1.0	0.7	$P < 0.0001$
C18 (Density of hair on back of leaf)	1.0–2.0	1.9	2.0–2.0	2.0	$P = 0.0657$
C19 (Density of hair on petiole)	1.0–2.0	1.4	0.0–2.0	1.2	$P = 0.2114$
C20 (Shape of leaf)	1.4–3.0	2.3	1.0–3.0	2.7	$P < 0.0001$
C21 (Density of hair on twig)	0.0–2.0	1.0	0.0–2.0	0.9	$P = 0.4407$

Group E corresponds to *P. bournei* and Group W to *P. zhennan*

inference when there is a large proportion of missing data (Roure et al., 2013). A rapid bootstrapping analysis with 100 bootstrap replicates was also undertaken. All data processing and phylogenetic analyses were carried out using the supercomputer at the Public Technology Service Center of XTBG, Chinese Academy of Sciences (Xishuangbanna, Yunnan, China).

2.3.4 Analyses of genetic structure

To determine how many genetic groups are present in the *P. bournei* and *P. zhennan* complex, the unlinked SNP matrix ($W_{clust} = 85\%$, $Min_{taxa} = 16$) was analyzed using fastStructure version 1.0 (Raj et al., 2014). We ran five replicates for each *K* value from 1 to 15 using the simple prior model. Then the number of clusters that best fit our data was determined by the utility "choose K.py: included in fastStructure and the clustering results were plotted by "distruct.py", which was also included in fastStructure.

To assess the genetic differentiation between putative groups, the AMOVA in Arlequin version 3.5 was employed (Excoffier & Lischer, 2010). The unlinked SNP matrix was used in the analysis. The analysis was undertaken for the two genetic groups (*P. bournei* and *P. zhennan*) identified in fastStructure (see Results).

2.4 Distribution and climate differentiation

Herbarium specimen location data from the Chinese Virtual Herbarium (CVH, http://www.cvh.ac.cn/), National Specimen Information Infrastructure (NSII, http://www.nsii.org.cn/), and the Global Biodiversity Information Facility (GBIF, http://www.gbif.org/) were combined with those from our sampling locations to refine the distribution areas of *P. bournei* and *P. zhennan*. After removing data for misidentified or duplicate specimens or spatially duplicated locations (occurrences with an average nearest-neighbor distance of <10 km), we recognized 123 putative records for *P. bournei* and 51 for *P. zhennan*. The Kernel density tool from the spatial analysis toolbox of ArcGIS version 10.2 (ESRI, 2011) was then used to estimate distribution areas for *P. bournei* and *P. zhennan*.

Climate data (~1950–2000, 2.5 arc-min) from the DIVA-GIS website (http://www.diva-gis.org/climate) (Hijmans et al., 2005) and 19 climatic values extracted for each record with DIVA-GIS version 7.5 (Hijmans et al., 2001; Table S4), were used for independent sample *t*-tests to compare interspecies differences for each climate variable. Principal component analysis of the 19 climate variables was also carried out using the Kaiser Criterion (Kaiser, 1960). Groupings observed in the scatter plot of the first two components were then evaluated further by discriminant analysis.

3 Results

3.1 Morphological analyses

Morphological cluster analysis resulted in two distinct groups (Group E and Group W, Fig. 2). Group E represented the 12 eastern localities: ZHH, SX, WY, YF, LY, YX, SCH, SHX, JH, FCH, RJ, and DY, with Group W representing samples from the 14 western localities: JK, WCH, LF, YCH, TL, XY, JY, CHN, SHF, YJ, QL, MSH, EM, and DJY (see Fig. 1). The independent sample *t*-test found that 10 characters differed significantly (Table 1, $P < 0.0001$) between the two groups, they were diameter of petiole (C1), length of petiole (C2), angle of leaf apex (C9), ratio of leaf length to width (C11), ratio of petiole length to

Table 2 Factor loadings and variances of 21 morphological characters based on 93 specimens of *Phoebe bournei* and *P. zhennan* in principal component analysis

Character	PC1	% var	PC2	% var	PC3	% var
Percent of variance		25.09		19.53		14.24
C1 (Diameter of petiole)	**−0.603**	1.62	0.385	1.03	−0.02	0.05
C2 (Length of petiole)	0.330	0.89	0.306	0.82	0.575	1.54
C3 (Length of leaf)	−0.273	0.73	0.845	2.27	−0.35	0.94
C4 (Length of leaf apex)	−0.457	1.23	0.637	1.71	0.053	0.14
C5 (Width of middle leaf)	0.193	0.52	0.902	2.42	0.216	0.58
C6 (Width of leaf)	0.263	0.71	0.898	2.41	0.165	0.44
C7 (Length from leaf base to width of leaf)	0.159	0.43	0.778	2.09	−0.52	1.40
C8 (Angle of leaf base)	−0.308	0.83	0.169	0.45	0.752	2.02
C9 (Angle of leaf apex)	**0.833**	2.24	0.253	0.68	0.200	0.54
C10 (Number of leaf's secondary vein)	−0.113	0.30	0.39	1.05	−0.06	0.16
C11 (C3/C6)	−0.627	1.68	−0.20	0.54	−0.58	1.56
C12 (C2/C1)	0.582	1.56	0.053	0.14	0.529	1.42
C13 (C7/C3)	0.754	2.03	0.055	0.15	−0.39	1.05
C14 (C9/C8)	0.802	2.15	0.059	0.16	−0.45	1.21
C15 (C4/C3)	−0.435	1.17	0.322	0.87	0.274	0.74
C16 (Resolution of tertiary veins)	**−0.634**	1.70	0.204	0.55	−0.04	0.11
C17 (Resolution of quaternary veins)	**−0.779**	2.09	0.097	0.26	−0.16	0.43
C18 (Density of hair on back of leaf)	0.320	0.86	0.015	0.04	0.242	0.65
C19 (Density of hair on petiole)	−0.226	0.61	−0.110	0.30	0.323	0.87
C20 (Shape of leaf)	0.519	1.39	0.095	0.26	−0.430	1.16
C21 (Density of hair on twig)	−0.128	0.34	−0.210	0.56	0.389	1.05

Bold text indicates the most distinctive characters among the directly measured characters. var, variance.

diameter (C12), length from leaf base to widest point/leaf length (C13), ratio of leaf apex angle to base angle (C14), resolution of tertiary veins (C16), resolution of quaternary veins (C17), and shape of leaf (C20). The first three principal components explained 25.09%, 19.53%, and 14.24% of the variation, respectively (Table 2, total 58.86%). These values were regarded as an acceptable cut-off level for visualization of the results based on the scree plot and Kaiser criterion (Kaiser, 1960; Cattell, 1966). The scatter plot also showed two clearly distinct groups (Fig. 3; Wilks' lambda = 0.113, $P < 0.0001$), corresponding to Groups E and W from the cluster analysis. These groups split mostly along PC1 and the absolute loading values of nine characters were larger than 0.5 (Table 2) in PC1, indicating that they were important in splitting the two groups. These characters were: diameter of petiole (C1), angle of leaf apex (C9), ratio of leaf length to width (C11), ratio of petiole length to diameter (C12), length from leaf base to widest point/leaf length (C13), ratio of leaf apex angle to base angle (C14), resolution of tertiary veins (C16), resolution of quaternary veins (C17), and shape of leaf (C20). Of these characters, C1, C9, C16, and C17 were the four most distinctive in distinguishing the two species according to absolute loading values in PCA (Table 2). *Phoebe bournei* has thicker petioles, narrower leaf, and more prominent tertiary and quaternary veins, compared to *P. zhennan* (Figs. 4, 5). The raw data for morphological analyses is deposited in the Dryad repository (Data S1).

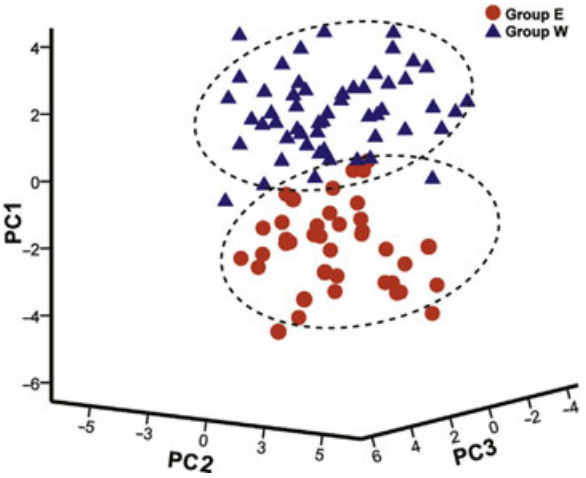

Fig. 3. Result of principal component analysis (PCA) of 21 morphological characters of 93 specimens. The PCA scatter plot of the first three coordinates shows the presence of two distinct groups: Group E, *Phoebe bournei* (orange circles); and Group W, *P. zhennan* (blue triangles).

3.2 Analyses of RAD-seq data

3.2.1 Restriction site-associated DNA sequencing and sequence data processing

A total of 631.53 million raw RAD sequences (per sample ranged from 7.61–25.06 million for the ingroup) were recovered and 427.7 million of these passed quality filtering (per sample, 6.88–25.04 million). The mean locus coverage depth varied among samples, partly due to degradation of some DNA samples (Table 3). The supermatrix contained 4 613 054 bp and included 56 395 loci and 325 984 SNPs, of which 50 858 were unlinked SNPs. The average proportion of missing data from the matrix was 14.99% (per sample, 9.24–24.01%), the average proportion of gaps was 4.15% (per sample, 0.95–5.24%), and GC content was relatively stable (per sample, 13.48–16.66%) (Table 3). The RAD-seq data are available on GenBank SRA (SRA accession: SRP145237; https://www.ncbi.nlm.nih.gov/sra/SRP145237). The supermatrix and unlinked SNP matrix

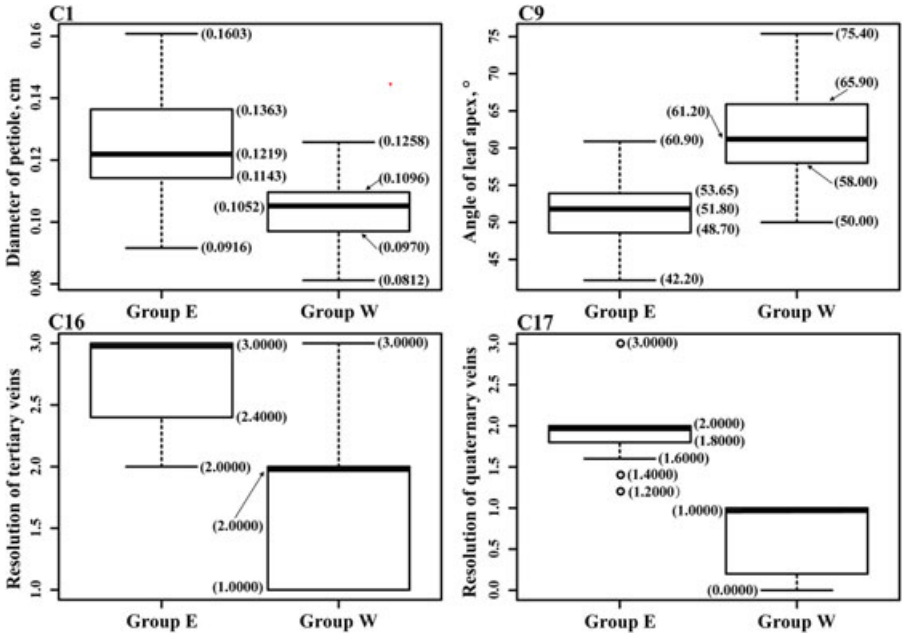

Fig. 4. Box and whisker plots of diameter of petiole (C1), angle of leaf apex (C9), and tertiary and quaternary veins (C16 and C17) of *Phoebe bournei* and *P. zhennan*. Thick horizontal bars within the boxes indicate the median, vertical lines indicate the upper and lower quartiles, and circles represent extreme values.

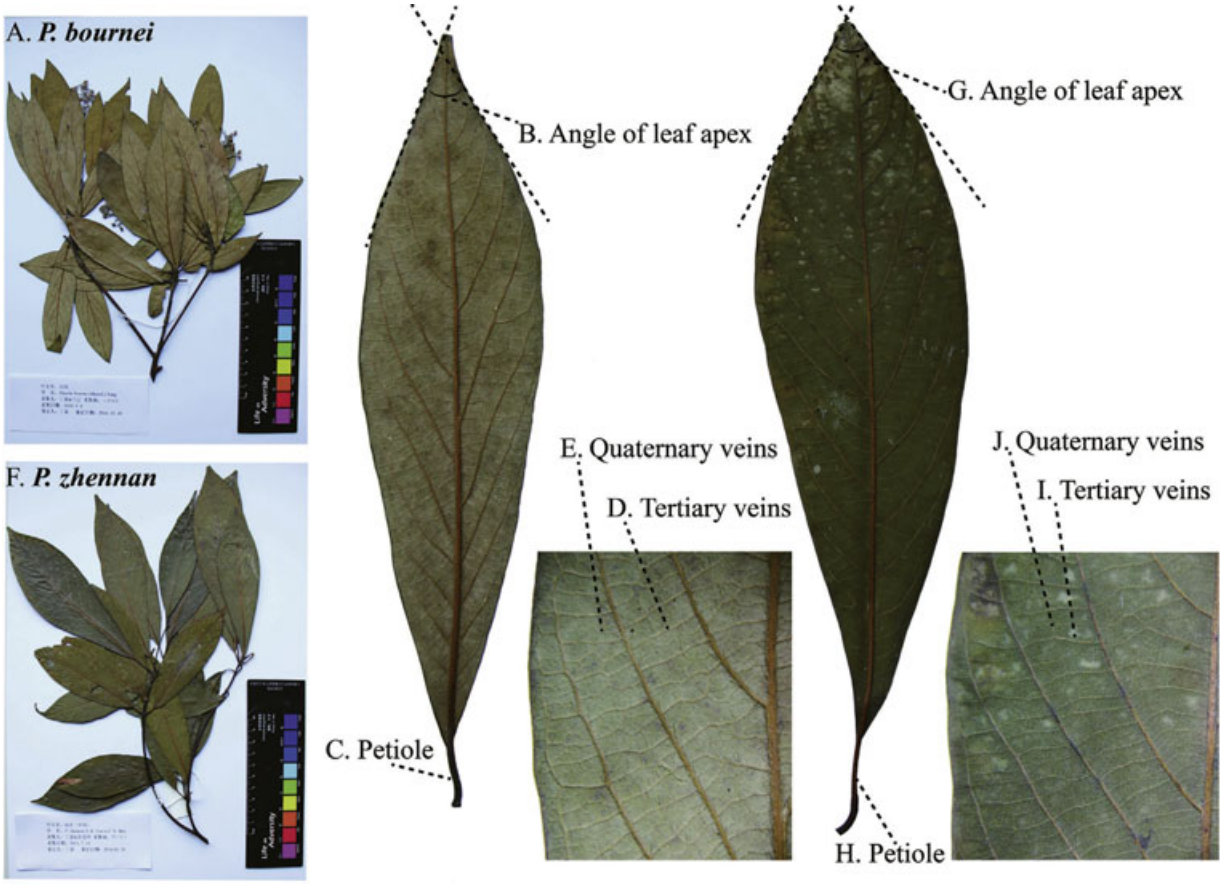

Fig. 5. Illustration of the four most distinctive morphological field characters to distinguish between *Phoebe bournei* (**A–E**) and *P. zhennan* (**F–J**). The angle of leaf apex (C1) in *P. zhennan* (**G**) was wider than that in *P. bournei* (**B**), the petiole (C2) of *P. bournei* (**C**) was thicker than that of *P. zhennan* (**H**), and the tertiary (C16) and quaternary veins (C17) in *P. bournei* (**D, E**) were more prominent than those of *P. zhennan* (**I, J**).

for the results presented below are deposited in the Dryad repository (Data S2).

3.2.2 Phylogenetic analyses

Maximum likelihood analysis divided the 26 individuals into two clades, corresponding to *P. bournei* (orange clade) and *P. zhennan* (blue clade), consistent with the two groups recovered in the morphology-based analyses, and both with 100% bootstrap support. However, two putative *P. bournei* individuals from northeastern Guizhou (JK and WCH) were clustered instead with *P. zhennan* (Fig. 6).

3.2.3 Analyses of genetic structure

The analysis of fastStructure found two genetic groups (the best *K* value was 2), corresponding to *P. bournei* and *P. zhennan* (Fig. 7). No cryptic genetic groups were discovered from the analyses with $K = 3$–15. Results for $K = 2$, 3, and 4 are presented here, all showing two genetic clusters (Fig. 7). The pattern of population structure identified with fastStructure was consistent with that of the ML analysis.

The results from AMOVA showed that the F_{st} between the two genetic groups (*P. bournei* and *P. zhennan*) identified by fastStructure was 0.338 ($P < 0.0001$), indicating that there is evident genetic differentiation between the two species. Of the total genetic variance, 33.8% was attributed to variation between the two species and 66.2% was from within species.

3.3 Distribution and climate differentiation

According to the estimation of distribution by the Kernel density tool in ArcGIS, *P. bournei* and *P. zhennan* are two parapatric species. *P. bournei* (123 records) occurs mainly in southeastern China (southern Zhejiang, Fujian, Jiangxi, Hunan, southwestern Hubei, northern Guangdong, northern Guangxi, southern Guizhou, and southeastern Chongqing), with dense distribution in the mountainous areas of central Fujian, southern Jiangxi, the Nanling Mountains, and the Wuling Mountains (Fig. 8A). In contrast, *P. zhennan* (51 records) comes from southwestern China (eastern Sichuan, Chongqing, southeastern Hubei, northern Guizhou, and northeastern Yunnan), mainly in the lowland and mountainous areas of the adjoining eastern regions of the Qionglai Mountains, the southern Sichuan hills, and the Wuling Mountains (Fig. 8B). The two species only overlapped in the Wuling Mountains at the transborder region of Hubei, Hunan, Guizhou, and Chongqing (Fig. 8C).

Climatic comparisons between the two species' localities suggested that precipitation was the most important variable affecting their distributions. Mean annual precipitation

Table 3 Number of raw restriction site-associated DNA (RAD) sequences, the number of RAD sequences >Q20, the mean coverage depths and the percentage of missing data, gaps, and GC percentage of samples in the terminal matrix

Sample ID	Location (all China)	Raw RAD sequences (million)	RAD sequences passed Q20 (million)	Coverage depth	Missing data (%)	Gaps (%)	Matrix GC (%)
Ingroup							
SX09	Shaxian, Fujian	16.34	14.68	11	13.71	5.07	15.27
ZHH06	Zhenghe, Fujian	16.60	14.91	13	13.29	5.09	15.34
WY12	Wuyuan, Jiangxi	15.41	13.83	20	12.48	5.12	15.48
YF13	Yifeng, Jiangxi	15.75	14.20	12	12.93	5.12	15.40
SCH08	Suichuan, Jiangxi	13.16	11.86	12	14.62	5.02	15.14
LY16	Liuyang, Hunan	12.13	10.79	9	16.52	4.92	14.79
YX06	Youxian, Hunan	14.61	13.06	16	13.62	5.08	15.28
JH02	Jiahe, Hunan	13.94	12.55	12	14.67	5.02	15.11
SHX18	Shixing, Guangdong	13.11	11.79	10	15.77	4.96	14.90
FCH02	Fuchuan, Guangxi	7.61	6.88	8	24.01	4.50	13.48
DY07	Duyun, Guizhou	12.10	10.91	10	18.35	4.82	14.47
RJ02	Rongjiang, Guizhou	13.73	12.44	13	15.5	4.97	14.94
JK05	Jiangkou, Guizhou	14.01	12.51	12	16.92	4.9	14.72
WCH11	Wuchuan, Guizhou	13.74	12.32	10	17.44	4.88	14.61
LF13	Laifeng, Hubei	19.84	17.89	16	13.54	5.06	15.30
TL02	Tongliang, Chongqing	23.43	23.41	18	9.24	1.99	16.66
YCH04	Yongchuan, Chongqing	24.73	24.71	18	11.01	0.95	16.50
JY08	Jiangyang, Sichuan	20.59	20.57	14	9.82	3.08	16.37
CHN70	Changning, Sichuan	17.31	17.29	11	12.27	3.01	15.91
XY13	Xuyong, Sichuan	21.18	21.16	13	11.92	1.94	16.16
EM69	E'mei, Sichuan	23.49	23.09	18	10.93	5.21	15.73
MSH15	Mingshan, Sichuan	25.06	25.04	15	11.56	3.02	16.01
QL31	Qionglai, Sichuan	24.47	24.07	16	11.85	5.16	15.56
DJY27	Dujiangyan, Sichuan	18.87	18.54	14	10.56	5.24	15.82
YJ13	Yanjin, Yunnan	201.20	20.10	15	11.17	3.03	16.09
SHF08	Shuifu, Yunnan	19.12	19.10	15	12.09	1.94	16.15
Outgroup							
CHJ03	Changjiang, Hainan	17.19	16.91	17	49.04	3.01	9.07

(BIO12) and precipitation of the wettest month (BIO13), driest month (BIO14), seasonality (BIO15), wettest quarter (BIO16), driest quarter (BIO17), and coldest quarter (BIO19) were all significantly higher for *P. bournei* than *P. zhennan* (Table S5, $P < 0.0001$).

The first two components of the climate PCA explained 37.5% and 27.72% of the variation (Table S6, total 65.22%) and this was regarded as an acceptable cut-off level for visualization of the results (Kaiser, 1960; Cattell, 1966). *Phoebe bournei* and *P. zhennan* occupied different climatic niches on the scatter plot with minimal overlap (Fig. 9; Wilks' lambda = 0.233, $P < 0.0001$). The localities mostly separated along PC1, with the three main PC1 climatic characters being precipitation of the driest month (BIO14), driest quarter (BIO17), and coldest quarter (BIO19) (Table S6). This further suggests that precipitation affects species distributions.

4 Discussion

4.1 Species delimitation and implications

Morphological cluster analysis and ordination (PCA) methods have been used for species delimitation in Lauraceae (*Machilus* Nees; Yang et al., 2002; Lin, 2003) and other taxa such as the *Taxus fuana* Nan Li & R. R. Mill complex (Taxaceae; Shah et al., 2008), *Microtoena insuavis* (Hance) Prain ex Briq. complex (Lamiaceae; Wang & Hong, 2011), and *Lemmaphyllum* C. Presl (Polypodiaceae; Wei & Zhang, 2013). We used 21 morphological characters in this study and they corroborated with RAD-seq data in separating two closely related species in *Lauraceae*, *Phoebe bournei* from *P. zhennan* (Figs. 6, 7).

These congruent molecular and morphological results support the recognition of two species, *P. bournei* and *P. zhennan*, based on a phylogenetic species concept (Nixon & Wheeler, 1990; Platnick & Wheeler, 2000). This result agrees with that of Lee et al. (1979), but disagrees with the concept of

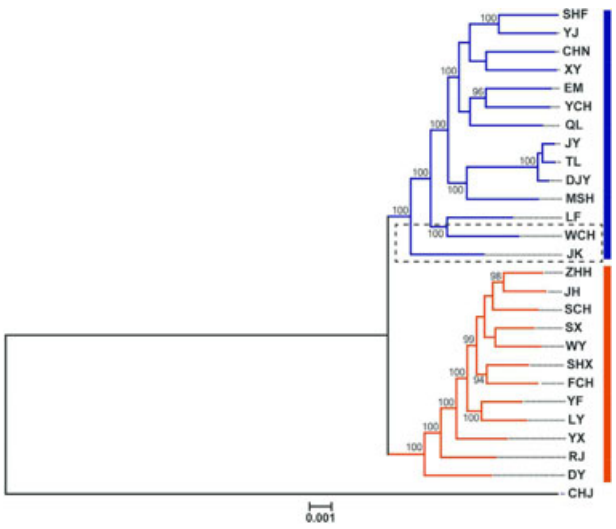

Fig. 6. Phylogenetic tree resulting from maximum likelihood analyses of the restriction site-associated DNA sequencing data matrix constructed using $W_{clust} = 85\%$ and $Min_{taxa} = 16$ and 26 individuals representing the 26 populations. In the dotted box, two putative *Phoebe bournei* individuals from northeastern Guizhou (JK and WCH) were clustered instead with *P. zhennan*. CHJ, Changjiang; CHN, Changning; EM, E'mei; DJY, Dujiangyan; DY, Duyun; FCH, Fuchuan; JH, Jiahe; JK, Jiangkou; JY, Jiangyang; LF, Laifeng; LY, Liuyang; MSH, Mingshan; QL, Qionglai; RJ, Rongjiang; SCH, Suichuan; SHF, Shuifu; SHX, Shixing; SX, Shaxian; TL, Tongliang; WCH, Wuchuan; WY, Wuyuan; XY, Xuyong; YCH, Yongchuan; YF, Yifeng; YJ, Yanjin; YX, Youxian; ZHH, Zhenghe.

a single variable species of Zou & Wu (1997). The 26 localities of the individuals sampled for RAD-seq represented largely the ranges for *P. bournei* and *P. zhennan* based on GIS data from specimen records (comparing Figs. 1, 8) and those reported by Li et al. (1982, 2008), except for two individuals of *P. bournei* from northeastern Guizhou (JK and WCH) which are clustered with samples of *P. zhennan* (Fig. 6). This finding indicates a new distribution record of *P. zhennan* in Guizhou.

Compared to traditional genetic sequence markers, RAD-seq uses a next generation sequencing platform to generate millions of short DNA fragments covering the genome (Baird et al., 2008; Davey et al., 2010), providing numerous loci informative in constructing phylogenies (Cariou et al., 2013; Gonen et al., 2015; Pante et al., 2015). In our study, delimitation between *P. bournei* and *P. zhennan* was clearly resolved by the RAD-seq data through phylogenetic and population genetic analyses (Figs. 6, 7; $F_{st} = 0.338$, $P < 0.0001$), further demonstrating the value of RAD-seq approach to taxonomic problem.

The integration of morphological and molecular data is a valuable approach in plant taxonomic and systematic studies (Dayrat, 2005; Padial et al., 2010). Although molecular analysis has recently been a popular method to delimitate taxa and evaluate phylogenetic relationships, our study again demonstrates the value of morphological analysis, which corroborates the molecular evidence in delineating *P. bournei* and *P. zhennan*.

4.2 Character differentiation and applications

Lee et al. (1979) considered four morphological characters as important for distinguishing *P. zhennan* from *P. bournei*: (i) branchlets densely villous; (ii) leaf blade elliptic; (iii) abaxial veinlets slightly distinct or invisible; and (iv) cymose panicles strongly patent. The current study supports only two of these as being diagnostic: the leaf blade of *P. zhennan* is elliptic to obovate-elliptic, whereas that of *P. bournei* is lanceolate (C20; Tables 1, 2); and the tertiary (C16) and quaternary veins (C17) in *P. bournei* (Figs. 5D, 5E) were more prominent than those of *P. zhennan* (Figs. 5I, 5J). However, the branchlets of *P. zhennan* were not evidently more villous and we found that the character "extension of cymose panicles" was ambiguous and apparently affected strongly by local growing conditions. Our study also found that the petioles (C1; Tables 1, 2) of *P. bournei* (Fig. 5C) are thicker than those of *P. zhennan* (Fig. 5H). Leaf shape also differs, with the angle of the leaf apex (C9; Tables 1, 2) being acuminate (wider) in *P. zhennan* (Fig. 5G) and acute in *P. bournei* (Fig. 5B).

Petiole diameter (C1), angle of leaf apex (C9), and the prominence of the tertiary and quaternary veins (C16 and C17) are probably the most convenient field characters to distinguish between the two species (Figs. 4, 5). Although the values of these four characters were also overlapping in ranges between the species, their means significantly differed (Table 1). In general, *P. bournei* has thicker petioles, narrower leaf, and more prominent tertiary and quaternary veins compared to *P. zhennan*, thus allowing for more sustainable management of gold-thread nanmu resources.

4.3 Climatic differentiation and geographic distribution

Climatic variables often determine plant distributions (Woodward, 1987; Pearson et al., 2002; Kozak et al., 2008), driving adaptation and changes of functional traits. One of the most obvious differences between *P. bournei* and *P. zhennan* is that the higher order veins of the former are distinct, whereas those of the latter are almost invisible (C16, C17; Tables 1, 2; Fig. 4). As a result, *P. bournei* has prominent abaxial veinlets whereas *P. zhennan* has tiny ones. This difference may be a result of adaptation to different climates (Roth-Nebelsick et al., 2001; Wright & Westoby, 2002; Boyce et al., 2009). Although *P. bournei* and *P. zhennan* occupy similar habitats, growing on fertile soils in ravines and along rivers below 1500 m in the EBLF of subtropical China (Li et al., 1982, 2008), *P. bournei* occurs in the eastern EBLF with higher precipitation owing to the stronger and wetter southeast monsoon from the Pacific Ocean. In contrast, *P. zhennan* grows in the western EBLF where it is influenced by the proportionally drier southwest monsoon from the Indian Ocean (Song, 1988; Wang et al., 2007) (Tables S5, S6). Consequently, *P. bournei* might be exposed to waterlogged conditions for longer periods and the more prominent veinlets might allow more efficient water transfer for stomatal release, relative to *P. zhennan*. This hypothesis can be tested by further investigation.

Historically, both *P. bournei* and *P. zhennan* were more widespread across their respective ranges (Lin, 1988), but because of long-term selective logging, deforestation, and environmental degradation, both species have now disappeared from many suitable habitats, leaving them scattered

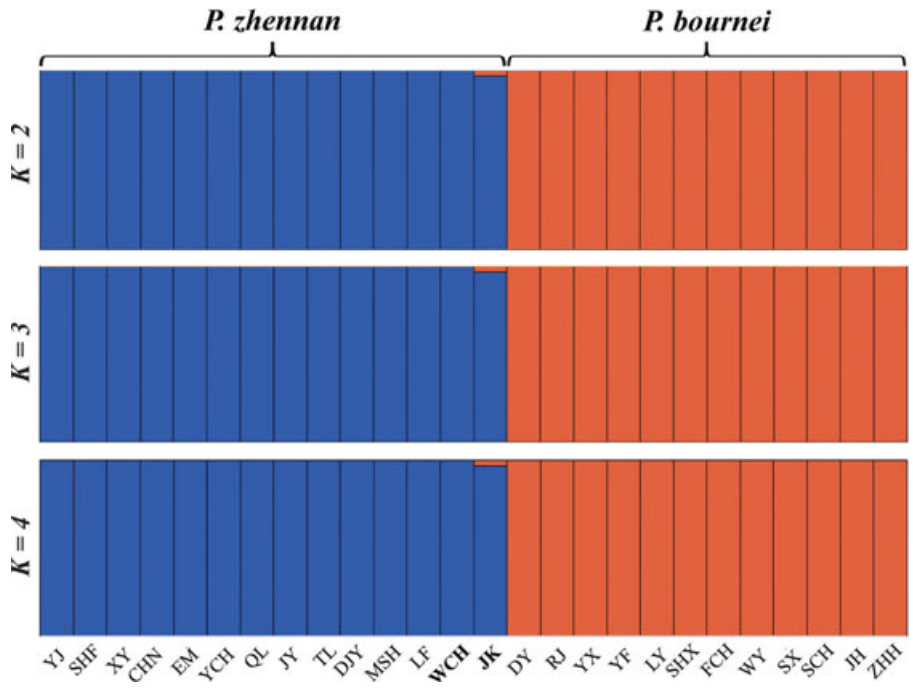

Fig. 7. Results from fastStructure analyses of the unlinked single nucleotide polymorphism data showing two genetic groups (*Phoebe bournei* and *P. zhennan*). This pattern remained the same in all analyses under models of $K = 2$ through 15. FastStructure determined that 2 was the best K value, thus the results of $K = 2$, 3, and 4 are shown. Bold locations (JK and WCH) represent two putative *P. bournei* individuals from northeastern Guizhou that were clustered instead with *P. zhennan*. CHJ, Changjiang; CHN, Changning; EM, E'mei; DJY, Dujiangyan; DY, Duyun; FCH, Fuchuan; JH, Jiahe; JK, Jiangkou; JY, Jiangyang; LF, Laifeng; LY, Liuyang; MSH, Mingshan; QL, Qionglai; RJ, Rongjiang; SCH, Suichuan; SHF, Shuifu; SHX, Shixing; SX, Shaxian; TL, Tongliang; WCH, Wuchuan; WY, Wuyuan; XY, Xuyong; YCH, Yongchuan; YF, Yifeng; YJ, Yanjin; YX, Youxian; ZHH, Zhenghe.

across the EBLF (Fig. 1). Both species are mainly confined to mountainous areas that have been suggested as the refugia of many plant species of subtropical China (Fig. 8) (Qiu et al., 2011; Liu et al., 2012). This evidence suggests the two species might have long survived in these areas.

4.4 Conservation and management

Accurate species delimitation coupled with a comprehensive knowledge of species distributions and ecological preferences are basic requirements for effective conservation and management (Li & Pritchard, 2009). The current study

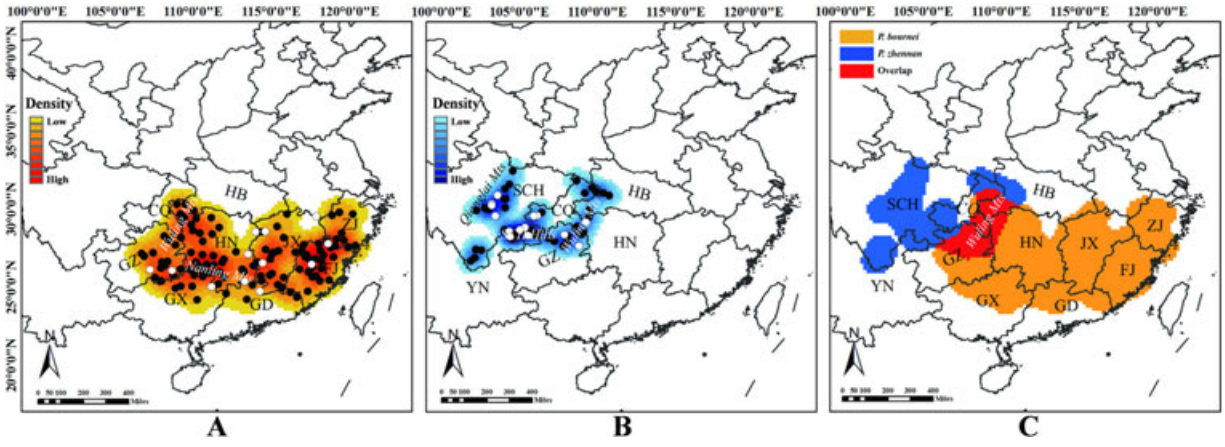

Fig. 8. Distributions of *Phoebe bournei* and *P. zhennan* based on occurrence records. The map is from the International Scientific and Technical Data Mirror Site, Computer Network Information Center, Chinese Academy of Sciences (http://www.gscloud.cn). **A,** Kernel density plot of *P. bournei*. **B,** Kernel density plot for *P. zhennan*. **C,** Distributions of *P. bournei* and *P. zhennan* based on the integration of **A** and **B**. Black circles represent records from herbarium specimens; white circles represent our field collections. CQ, Chongqing; FJ, Fujian; GD, Guangdong; GX, Guangxi; GZ, Guizhou; HB, Hubei; HN, Hunan; JX, Jiangxi; SCH, Sichuan; S SCH Hills, southern Sichuan hills; YN, Yunnan; ZJ, Zhejiang.

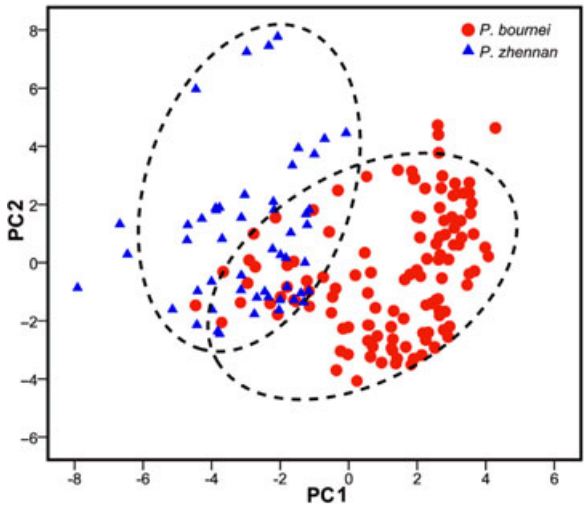

Fig. 9. Principal component analyses (PCA) of 19 climate variables. PCA scatter plot of the first two coordinates of a climate-based analysis of gold-thread nanmu localities showed that *Phoebe bournei* and *P. zhennan* largely occupied different climatic niches despite having some geographic overlap.

provided critical information for the conservation and sustainable management of the two most important gold-thread nanmu tree species. We also identified the most obvious morphological differences for the field recognition and clarified the geographic distributions of the two species.

Central Fujian, southern Jiangxi, the Nanling Mountains, and Wuling Mountains are centers of distribution of *P. bournei* (abundant); the adjoining eastern regions of the Qionglai Mountains, southern Sichuan hills, and Wuling Mountains contain the best remnants of *P. zhennan*. These should be the priority of conservation areas. Given the high price of gold-thread nanmu timber, current bans on the felling of source *Phoebe* species to prevent their continuing decline, together with tough penalties for illegal felling, should continue, especially for *P. bournei* and *P. zhennan*. Given that gold-thread nanmu tree species have an extremely slow growth rate, sustainable forestry practices need to be developed.

Acknowledgements

We thank the forestry departments and nature reserves from the provinces and municipalities of Chongqing, Fujian, Guangdong, Guangxi, Guizhou, Hubei, Hunan, Jiangxi, Sichuan, Yunnan, and Zhejiang for their support and coordination of the fieldwork. We also thank J. F. Huang, H. H. Meng, H. Ma, and W. M. Xu for laboratory assistance. Special thanks go to Hsi Wen Li for identifying some difficult specimens. This study was supported by the Science and Technology Basic Resources Investigation Program of China: Survey and Germplasm Conservation of Plant Species with Extremely Small Populations in South-west China (2017FY100100), the Yunnan Provincial Science and Technology Department, China (2017FB033), the National Natural Science Foundation of China (31370245), Biodiversity Conservation Program of the Chinese Academy of Sciences (ZSSD-013), and the 135 Program of the Chinese Academy of Sciences (XTBG-F04). Special thanks to the anonymous reviewers and the handling editor for their critical comments and help in improving the manuscript.

References

Baird NA, Etter PD, Atwood TS, Curry MC, Shiver AL, Lewis ZA, Selker EU, Cresko WA, Johnson EA. 2008. Rapid SNP discovery and genetic mapping using sequenced RAD markers. *PLoS One* 3: e3376.

Boucher FC, Casazza G, Szovenyi P, Conti E. 2016. Sequence capture using RAD probes clarifies phylogenetic relationships and species boundaries in *Primula* sect. *Auricula*. *Molecular Phylogenetics and Evolution* 104: 60–72.

Boyce KC, Brodribb TJ, Field TS, Zwienieck MA. 2009. Angiosperm leaf vein evolution was physiologically and environmentally transformative. *Proceedings of the Royal Society B: Biological Sciences* 276: 1771–1776.

Cariou M, Duret L, Charlat S. 2013. Is RAD-seq suitable for phylogenetic inference? An *in silico* assessment and optimization. *Ecology and Evolution* 3: 846–852.

Cattell RB. 1966. The scree test for the number of factors. *Multivariate Behavioural Research* 1: 245–276.

Chen YZ. 2013. Cultural history and modern life of gold-thread nanmu. *Light Industry Science and Technology* 12: 96–114. (in Chinese)

Cheng WC. 1983. Lauraceae. In: Cheng WC ed. *Sylva of China. Beijing*: China Forestry Publishing Press. 1: 606–877. (in Chinese)

Davey JW, Davey JL, Blaxter ML, Blaxter MW. 2010. RAD-seq: Next-generation population genetics. *Briefings in Functional Genomics* 9: 416–423.

Dayrat B. 2005. Towards integrative taxonomy. *Botanical Journal of the Linnean Society* 85: 407–415.

Eaton DAR. 2014. PyRAD: Assembly of de novo RAD-seq loci for phylogenetic analyses. *Bioinformatics* 30: 1844–1849.

Eaton DAR, Ree RH. 2013. Inferring phylogeny and introgression using RAD-seq data: An example from flowering plants (*Pedicularis*: Orobanchaceae). *Systematic Biology* 62: 689–706.

Escudero M, Eaton DA, Hahn M, Hipp AL. 2014. Genotyping-by-sequencing as a tool to infer phylogeny and ancestral hybridization: A case study in *Carex* (Cyperaceae). *Molecular Phylogenetics and Evolution* 79: 359–367.

ESRI. 2011. ArcGIS desktop: Release 10. Redlands: Environmental Systems Research Institute.

Etter PD, Bassham S, Hohenlohe PA, Johnson EA, Cresko WA. 2011. SNP discovery and genotyping for evolutionary genetics using RAD sequencing. In: Orgogozo V, Rockman MV eds. *Molecular methods for evolutionary genetics*. New York: Springer. 157–158.

Excoffier L, Lischer HEL. 2010. Arlequin suite version 3. 5: A new series of programs to perform population genetics analyses under Linux and Windows. *Molecular Ecology Resources* 10: 564–567.

Fu LG, Jin JM. 1991. *The China plant red data book, volume I: Rare and endangered plants*. Beijing: Science Press. (in Chinese)

Fitz-Gibbon S, Hipp AL, Pham KK, Manos PS, Sork VL. 2017. Phylogenomic inferences from reference-mapped and de novo assembled short-read sequence data using RAD-seq sequencing of California white oaks (*Quercus* section *Quercus*). *Genome* 60: 743–755.

Gao JH, Zhang W, Li JY, Long HL, He W, Li XQ. 2016. Amplified fragment length polymorphism analysis of the population

structure and genetic diversity of *Phoebe zhennan* (Lauraceae), a native species to China. *Biochemical Systematics and Ecology* 64: 149–155.

Gonen S, Bishop SC, Houston RD. 2015. Exploring the utility of cross-laboratory RAD-sequencing datasets for phylogenetic analysis. *BMC Research Notes* 8: 299.

Hijmans RJ, Guarino L, Cruz M, Rojas E. 2001. Computer tools for spatial analysis of plant genetic resources data: 1. DIVA-GIS. *Plant Genetic Resources Newsletter* 127: 15–19.

Hijmans RJ, Cameron SE, Parra JL, Jones PG, Jarvis A. 2005. Very high resolution interpolated climate surfaces for global land areas. *International Journal of Climatology* 25: 1965–1978.

Hipp AL, Eaton DA, Cavender-Bares J, Fitzek E, Nipper R, Manos PS. 2014. A framework phylogeny of the American oak clade based on sequenced RAD data. *PLoS One 9: e* 93975.

IUCN. 2017. The IUCN red list of threatened species. Version 2017-3. Available from http://www.iucnredlist.org/ [accessed 5 December 2017].

Jia X, Huang QS, Liu GH, Li JX, Liao JH, Sun JC. 2014. The present status of Phoebe zhennan. *Chinese Horticulture Abstracts* 10: 55–59.

Kaiser HF. 1960. The application of electronic computers to factors analysis. *Educational and Psychological Measurement* 20: 141–151.

Kozak KH, Graham CH, Wiens JJ. 2008. Integrating GIS-based environmental data into evolutionary biology. *Trends in Ecology and Evolution* 23: 141–148.

Lee SK, Wei FN, Wei YZ, Li HW. 1979. Materiae ad floram Lauracearum sinicarum (III). *Acta Phytotaxonomica Sinica* 17: 45–74. (in Chinese)

Li DL, Jin YQ, Xiang QB. 2004. The geographical distribution, research status and developmental utilization prospect of *Phoebe* Nees plant resource of our country. *Journal of Fujian Forestry Science and Technology* 32: 5–9. (in Chinese)

Li DZ, Pritchard HW. 2009. The science and economics of ex situ plant conservation. *Trends in Plant Science* 14: 614–621.

Li HW, Pai PY, Li YR, Lee SK, Wei FN, Wei YZ, Yang YC, Huang PH, Tsui HP, Shia ZD, Li JL. 1982. Lauraceae. In: *Flora Reipublicae Popularis Sinicae*. Beijing: Science Press. 31: 1–463.

Li HW, Li J, Huang PH, Wei FN, Cui HB, van der Werff H. 2008. Lauraceae. In: Wu ZY, Raven PH, Hong DY eds. *Flora of China*. Beijing: Science Press; St. Louis: Missouri Botanical Garden Press. 7: 102–254.

Li L, Li J, Rohwer JG, van der Werff H, Wang ZH, Li HW. 2011. Molecular phylogenetic analysis of the *Persea* group (Lauraceae) and its biogeographic implications on the evolution of tropical and subtropical amphi-Pacific disjunctions. *American Journal of Botany* 98: 1–17.

Lin HR. 1988. The ancient nanmu and its changing distribution. *Forestry Science and Technology* 9: 48–58. (in Chinese)

Lin XZ. 2003. *The systematical studies on species from genus* Machilus *in Zhejiang province*. Ph. D. Dissertation. Beijing: Beijing Forestry University. (in Chinese)

Liu JQ, Sun YS, Ge XJ, Gao LM, Qiu YX. 2012. Phylogeographic studies of plants in China: Advances in the past and directions in the future. *Journal of Systematics and Evolution* 50: 267–275.

Miller MR, Dunham JP, Amores A, Cresko WA, Johnson EA. 2007. Rapid and cost-effective polymorphism identification and genotyping using restriction site associated DNA (RAD) markers. *Genome Research* 17: 240–248.

Milligan GW. 1980. An examination of the effect of six types of error perturbation on fifteen clustering algorithms. *Psychometrika* 45: 325–342.

Nixon KC, Wheeler QD. 1990. An amplification of the phylogenetic species concept. *Cladistics* 6: 211–223.

Padial JM, Miralles A, De la Riva I, Vences M. 2010. Review: The integrative future of taxonomy. *Frontiers in Zoology* 7: 16.

Pante E, Abdelkrim J, Viricel A, Gey D, France S, Boisselier MC, Samadi S. 2015. Use of RAD sequencing for delimiting species. *Heredity* 114: 450–459.

Pearson RG, Dawson TP, Berry PM, Harrison PA. 2002. SPECIES: A spatial evaluation of climate impact on the envelope of species. *Ecological Modelling* 154: 289–300.

Platnick NI, Wheeler Q. 2000. A defense of the phylogenetic species concept (sensu Wheeler and Platnick). In: Wheeler Q, Meier R eds. *Species concepts and phylogenetic theory: A debate*. New York: Columbia University Press. 185–197.

Qi ZC, Yu Y, Liu X, Pais A, Ranney T, Whetten R, Xiang QY. 2015. Phylogenomics of polyploidy *Fothergilla* (Hamamelidaceae) by RAD-tag based GBS – Insights into species origin and effects of software pipelines. *Journal of Systematics and Evolution*: 53: 432–447.

Qiu YX, Fu CX, Comes HP. 2011. Plant molecular phylogeography in China and adjacent regions: Tracing the genetic imprints of Quaternary climate and environmental change in the world's most diverse temperate flora. *Molecular Phylogenetics and Evolution* 59: 225–244.

Raj A, Stephens M, Pritchard JK. 2014. fastSTRUCTURE: Variational inference of population structure in large SNP data sets. *Genetics* 197: 573–589.

Ree RH, Hipp AL. 2015. Inferring phylogenetic history from restriction site associated DNA (RAD-seq). In: Hörandl E, Appelhans MS eds. *Next-generation sequencing in plant systematics*. Bratislava: IAPT. 181–204.

Rogers SO, Bendich AJ. 1988. Extraction of DNA from plant tissues. *Plant Molecular Biology* 6: 1–10.

Roth-Nebelsick A, Uhl D, Mosbrugger V, Kerp H. 2001. Evolution and function of leaf venation architecture: A review. *Annals of Botany* 87: 553–566.

Roure B, Baurain D, Philippe H. 2013. Impact of missing data on phylogenies inferred from empirical phylogenomic data sets. *Molecular Biology and Evolution* 30: 197–214.

Rubin BER, Ree RH, Moreau CS. 2012. Inferring phylogenies from RAD sequence data. *PLoS ONE* 7: e33394.

Shah A, Li DZ, Moller M, Gao LM, Hollingsworth ML, Gibby M. 2008. Delimitation of *Taxus fuana* Nan Li & R. R. Mill (Taxaceae) based on morphological and molecular data. *Taxon* 57: 211–222.

Song Y, Yao X, Tan YH, Gan Y, Yang JB, Corlett RT. 2017. Comparative analysis of complete chloroplast genome sequences of two subtropical trees, *Phoebe sheareri* and *Phoebe omeiensis* (Lauraceae). *Tree Genetics & Genomes* 13: 120.

Song YC. 1988. The essential characteristics and main types of the broad-leaved evergreen forest in China. *Phytocoenologia* 16: 105–123.

Stamatakis A. 2014. RAxML version 8: A tool for phylogenetic analyses and post analysis of large phylogenies. *Bioinformatics* 30: 1312–1313.

Takahashi T, Moreno E. 2015. A robust phylogeny among major lineages of the East African cichlids. *Molecular Phylogenetics and Evolution* 93: 307–317.

Takahashi T, Sota T. 2016. A robust phylogeny among major lineages of the East African cichlids. *Molecular Phylogenetics and Evolution* 100: 234–242.

Takahashi T, Nagata N, Sota T. 2014. Application of RAD-based phylogenetics to complex relationships among variously related taxa in a species flock. *Molecular Phylogenetics and Evolution* 80: 137–144.

Tripp EA, Tsai YE, Zhuang YB, Dexter KG. 2017. RAD-seq dataset with 90% missing data fully resolves recent radiation of *Petalidium* (Acanthaceae) in the ultra-arid deserts of Namibia. *Ecology and Evolution* 7: 7920–7936.

Wagner CE, Keller I, Wittwer S, Selz OM, Mwaiko S, Greuter L, Sivasundar A, Seehausen O. 2013. Genome-wide RAD sequence

data provide unprecedented resolution of species boundaries and relationships in the Lake Victoria cichlid adaptive radiation. *Molecular Ecology* 22: 787–798.

Wang Q, Hong DY. 2011. Character analysis and taxonomic revision of the *Microtoena insuavis* complex (Lamiaceae). *Botanical Journal of the Linnean Society* 165: 315–327.

Wang S, Xie Y. 2004. Chapter 6: China species red list, Lauraceae. In: Wang S, Xie Y eds. *China species red list*. Beijing: Higher Education Press. 1: 330–334. (in Chinese)

Wang XH, Kent M, Fang XF. 2007. Evergreen broad-leaved forest in Eastern China: Its ecology and conservation and the importance of resprouting in forest restoration. *Forest Ecology and Management* 245: 76–87.

Wang XQ, Zhao L, Eaton DAR, Li DZ, Guo ZH. 2013. Identification of SNP markers for inferring phylogeny in temperate bamboos (Poaceae: Bambusoideae) using RAD sequencing. *Molecular Ecology Resources* 13: 938–945.

Wei XP, Zhang XC. 2013. Species delimitation in the fern genus *Lemmaphyllum* (Polypodiaceae) based on multivariate analysis of morphological variation. *Journal of Systematics and Evolution* 51: 485–496.

Woodward FI. 1987. *Climate and plant distribution*. Cambridge: Cambridge University Press.

Wright IJ, Westoby M. 2002. Leaves at low versus high rainfall: Coordination of structure, lifespan and physiology. *New Phytologist* 155: 403–416.

Yang SY, Chen MY, Yang JT. 2002. Application of cecidomyiid galls to the systematics of the genus *Machilus* (Lauraceae) in Taiwan. *Botanical Bulletin of Academia Sinica* 43: 31–35.

Yang YC. 1945. New species, varieties and combinations of Lauraceous plants. *Journal of the West China Border Research Society* 70–88.

Zou HY, Wu DR. 1997. Taxonomic notes of *Phoebe bournei*. In: Zou HY, Wu DR eds. *Population ecology of bourne Phoebe (Phoebe bournei)*. Beijing: China Forestry Publishing Press. 2–4. (in Chinese)

Supplementary Material

The following supplementary material is available online for this article at http://onlinelibrary.wiley.com/doi/10.1111/jse.12433/suppinfo:

Fig. S1. Illustration of the characters used in the morphological analyses of Phoebe bournei and *P. zhennan*.

Table S1. Vouchers used in the morphological or restriction site-associated DNA sequencing analyses of *Phoebe bournei* and *P. zhennan*. The robust vouchers were used in restriction site-associated DNA sequencing analyses.

Table S2. Number, locality, coordinates, and altitude of the samples of *Phoebe bournei* and *P. zhennan* used in the restriction site-associated DNA sequencing analyses.

Table S3. Twenty-one morphological characters used in the morphological analyses of *Phoebe bournei* and *P. zhennan*.

Table S4. Nineteen climate variables for the time period 1950–2000 from the WorldClim database.

Table S5. Value ranges, mean values, and *t*-test results of 19 climate variables of 123 records of *Phoebe bournei* and 51 records of *P. zhennan* extracted by DIVA-GIS 7.5.

Table S6. Character ranks of the 19 climate variables, determined by the product between the first two components values and proportion of variance for each axis. Climate variables shown in bold were the most distinctive ones between *P. bournei* and *P. zhennan*.

Data S1. Raw data for morphological analyses, available from the Dryad Digital Repository: https://doi.org/10.5061/dryad.1k8738h

Data S2. Supermatrix for phylogenetic analyses and unlinked single nucleotide polymorphism matrix for the analyses of genetic structure, available from the Dryad Digital Repository: https://doi.org/10.5061/dryad.1k8738h